International Journal of Power Electronics and Drive Systems (IJPEDS)
Vol. 13, No. 4, December 2022, pp. 2541~2554
ISSN: 2088-8694, DOI: 10.11591/ijpeds.v13.i4.pp2541-2554

Power oscillation damping control using PI-neuron network controller for distributed generator grid connection with MVDC

Kittaya Somsai[1], Nakarin Sripanya[1], Chaiyut Sumpavakup[2]
[1]Department of Electrical Engineering, Faculty of Industry and Technology, Rajamangala University of Technology Isan, Sakon Nakhon, Thailand
[2]Research Centre for Combustion Technology and Alternative Energy-CTAE and College of Industrial Technology, King Mongkut's University of Technology North Bangkok, Bangkok, Thailand

Article Info

Article history:

Received Mar 14, 2022
Revised Jul 27, 2022
Accepted Aug 10, 2022

Keywords:

Distributed generator
Grid connection
MVDC
Neural network
Power oscillation

ABSTRACT

Distributed generator (DG) connection to the system with the DC grid called medium voltage direct current (MVDC) grid connection has received attention and gradually integrated into the distribution grid. The linear controller, such as the PI controller, usually uses the MVDC grid control for power oscillation damping. The PI controller is limited and does not show satisfactory results when the load and parameters of the system itself are changed. This paper proposes the PI with neuron network (NN) as a feed-forward controller (PINNF) to improve the control of the DG grid connection with the MVDC. The proposed PINNF controller is applied to control the power oscillation damping. Since the NN can estimate the proper feed-forward control signals in each situation to the control system, the proposed PINNF controller performs better than the conventional PI controller. The effectiveness of the proposed PINNF controller is validated using nonlinear dynamic simulations on the MATLAB/Simulink program. Four case tests are presented and discussed in this paper. Results indicate the improvement of power oscillation damping stability and performance in the MVDC grid connection with the proposed PINNF controller.

Corresponding Author:

Kittaya Somsai
Department of Electrical Engineering, Faculty of Industry and Technology
Rajamangala University of Technology Isan
Sakon Nakhon Campus, 47160, Thailand
Email: kittaya.so@rmuti.ac.th

1. INTRODUCTION

Distributed power generation technology has been developed to support distributed energy sources in many areas. The advantage of distributed power generation in terms of power management and distribution is that it distributes power generation that allows the power system to have a two-way flow [1]. The DGs are usually small sets of synchronous generators ranging from a few kilowatts to tens of megawatts designed, installed, and operated in a distribution network [2]. However, connecting the DG to the system has more stringent user conditions and requirements for power quality that traditional AC distribution networks may not be able to support [3], [4]. The power oscillation problem due to the inertia of the synchronous generator is another quality issue that has been a concern for DG connections [5]–[7]. The oscillation is observed while the synchronous DG is connected to the system. Therefore, the oscillation problem is essential and may lead to not continuing operations to connect the synchronization DG in the power system [8].

In the transmission system, the high voltage direct current (HVDC) transmission line and the flexible AC transmission systems (FACTS) family with power oscillation damping mod has been popularly applied to power grids to improve the power oscillation [9]–[11]. Since the HVDC and FACTS include the main part with the Voltage Source Converter (VSC) that has the advantage of independent and fast control of active and reactive powers, the power oscillation can be controlled. Concurrently, a similar smaller-scale technology called medium voltage direct current (MVDC) has been interested and gradually integrated into the distribution grid. The integration of DG on many different levels of the system offers potential benefits relying on MVDC technology compared to traditional AC systems [12]. Figure 1 shows the MVDC grid connection with a small 5MW DG synchronous generator connected to the DC bus. The MVDC grids have a better transfer capacity, flexibility, controllability, and power supply reliability. The MVDC is gaining more attention for distribution in power systems, mainly used successfully between distribution grids [13]–[15], where it can be used for various renewable power sources.

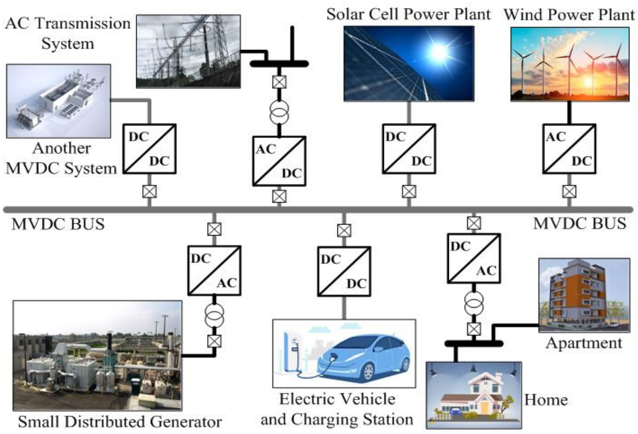

Figure 1. Schematic diagram grid connection with MVDC system

There are several applications of the MVDC in the distribution system [16], [17]. Joseph *et al.*, [16] proposed MVDC link between the mainland in North Wales and the island of Anglesey, while the MVDC and Grid Interties applications are presented in [17]. The MVDC in DC microgrid application is illustrated in [18], covering AC interfaces, architectures, possible grounding schemes, power quality issues, and communication systems. Furthermore, the MVDC is introduced to improve the power oscillation damping of the DG grid connection, as presented in [12] and [19]. Therefore, to improve the power oscillation of the DG connection, the MVDC grid connection is proposed and investigated in this paper.

However, the DG grid connection with the MVDC is a nonlinear system, leading to being hard to determine adequate parameters and design the control. The linear control theory is proposed based on the linear approximation technique [20] for analyzing and designing the control system. The PI controller is the linear controller popularly used with the rotating reference frames using Park transformation, a widespread technique popularly applied to control various VSCs, as illustrated in [21]–[22]. Mehmood *et al.*, [23] proposes a double-closed-loop control topology based on the rotating reference frames with the PI controller to control the MVDC. Therefore, the PI controller based on the rotating reference frames is used in this paper.

Although PI controller is generally applied to MVDC control, it is linear and symmetric. So, it has limitations for highly nonlinear systems. The PI controller is designed using a linear model, often obtained by linearization at specific operating conditions. It is limited when a defined boundary is unavailable or may not perform well when it is used outside a particular boundary. In addition, the PI controller has the overshoots and undershoots in the control system's output, and its parameters must be adjusted if the load and the system itself are changed. Hence, tuning and optimizing this controller is challenging and complex, particularly under varying load conditions, parameter changes, and abnormal modes of operation [24]. The performance of the VSC with the PI controller to parameter variations and uncertainties can be significantly increased with the help of feed-forward control, as shown in [25], [26]. However, the feed-forward control signals of those studies are obtained by measurement and calculation with the system's parameters that variations and uncertainties so that it does not give satisfactory results when the parameters of the system itself are changed. This problem can be mitigated by using the NN to estimate the proper feed-forward control signals in each situation to the control system.

The NN of living things inspires many technologies. Researchers from many disciplines have designed NN to solve pattern recognition, prediction, optimization, and control systems [27]-[30]. The NN can operate beyond a defined boundary and become an alternative solution for control systems. Controllers based on NN principles benefiting from the learning capabilities of NN are suitable for adaptive controls where the controller needs to adapt to environmental changes. The application of the NN to damp power oscillation is shown in [31], and the results show that the NN can emulate nonlinear dynamics and show a promising robust nonlinear performance.

This paper presents the study of the DG with MVDC grid connection on the distribution system to solve traditional AC connection problems. This study focuses on the MVDC control to solve power quality in the event of power oscillation at the connection point of the DG. The conventional PI controller and the proposed PINNF controller are tested and compared. The four case tests are implemented by MATLAB/Simulink program simulation.

2. MODELING OF DISTRIBUTION GENERATOR GRID CONNECTION WITH MVDC

This paper presents the DG grid connection with the MVDC. The schematic diagram is shown in Figure 2. It consists of three parts: 1) the DG and local load 2, 2) the MVDC, and 3) the Utility Electrical Power Station (EPS) and local load 1. In part 1, the DG is connected to the MVDC through the step-up transformer. At this point, the local load 2 has been installed. This part is called DG ZONE. The MVDC in part 2 consists of two connected back-to-back VSCs with a common DC link voltage. Two VSCs have to be connected to the AC system with the interface impedances so that the interface impedances can function as the AC filter for VSC. The last one, part 3, consists of the EPS and local load 1. This part is directly connected to the MVDC. The equivalent circuit of distributed generator grid connection with MVDC is shown in Figure 3. In this figure, the load is modeled by a series of resistance and inductance. Simplification assumes that the source, load, and MVDC are balanced. By applying the *abc*-to-*dq* transformation, the mathematical model of the system can be obtained, as shown in (1)-(16).

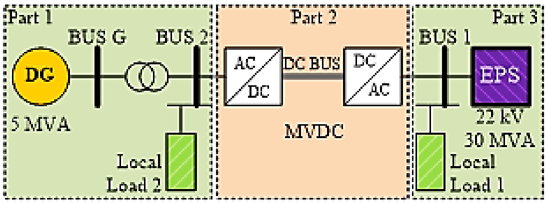

Figure 2. Schematic diagram of distributed generator grid connection with MVDC

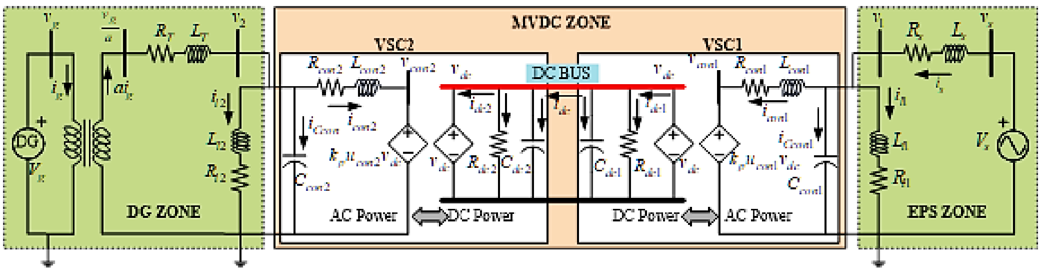

Figure 3. Equivalent circuit of distributed generator grid connection with MVDC

2.1. Mathematical of DG ZONE

In this paper, the three-phase salient-pole synchronous generator is used. The dynamic model of the generator referring to the rotor reference frame can be expressed in [32]. The (1)-(2) are the stator voltage equations, and the (3)-(6) are the rotor voltage equations, while the relationship between the torque and rotor speed can be written as shown in (7).

$$\frac{d\lambda_{qs}^r}{dt} = v_{qs}^r + r_s i_{qs}^r - \omega_r \lambda_{ds}^r \tag{1}$$

$$\frac{d\lambda^{r}_{ds}}{dt}=v^{r}_{ds}+r_s i^{r}_{ds}+\omega_r\lambda^{r}_{qs} \quad (2)$$

$$\frac{d\lambda'^{r}_{kq1}}{dt}=v'^{r}_{kq1}-r'_{kq1}i'^{r}_{kq1} \quad (3)$$

$$\frac{d\lambda'^{r}_{kq2}}{dt}=v'^{r}_{kq2}-r'_{kq2}i'^{r}_{kq2} \quad (4)$$

$$\frac{d\lambda'^{r}_{fd}}{dt}=v'^{r}_{fd}-r'_{fd}i'^{r}_{fd} \quad (5)$$

$$\frac{d\lambda'^{r}_{kd}}{dt}=v'^{r}_{kd}-r'_{kd}i'^{r}_{kd} \quad (6)$$

$$\frac{d\omega_r}{dt}=\frac{P}{2J}(T_m-T_e) \quad (7)$$

Where

$$T_e=\frac{3}{2}\frac{P}{2}(\lambda^{r}_{ds}i^{r}_{qs}-\lambda^{r}_{qs}i^{r}_{ds}) \quad (8)$$

In the above equations, the λ^{r}_{ds} and λ^{r}_{qs} represent the stator flux linkages in *dq* axes, and the r_s is the stator winding resistance. The v^{r}_{ds} and v^{r}_{qs} are the generator output voltages in *dq* axes, whereas the output currents in *dq* axes are represented by i^{r}_{ds} and i^{r}_{qs}. The rotor flux linkages of three damper winding are represented by λ'^{r}_{kd}, λ'^{r}_{kq1} and λ'^{r}_{kq2}, and the flux linkage of field winding is represented by λ'^{r}_{fd}. The resistances of three damper windings are r'_{kd}, r'_{kq1} and r'_{kq2}, and the resistance of field winding is r'_{fd}. The v'^{r}_{kd}, v'^{r}_{kq1} and v'^{r}_{kq2} are the voltage of three damper windings, and the v'^{r}_{fd} is the field winding voltage. The ω_r is rotor speed used as the reference frame speed or the reference frame fixed in the rotor. The input and electromagnetic torque in the rotor reference frame are T_m and T_e, respectively. Where *J* is the rotor's inertia, while *P* is the number of poles in the machine.

The currents (i^{r}_{qs}, i^{r}_{ds}, i'^{r}_{kq1}, i'^{r}_{kq2}, i'^{r}_{kd} and i'^{r}_{fd}) in the (1)-(6) can be obtained by using (9).

$$\begin{bmatrix}\lambda^{r}_{qs}\\ \lambda^{r}_{ds}\\ \lambda'^{r}_{kq1}\\ \lambda'^{r}_{kq2}\\ \lambda'^{r}_{fd}\\ \lambda'^{r}_{kd}\end{bmatrix}=\begin{bmatrix}-(L_{ls}+L_{mq}) & 0 & L_{mq} & L_{mq} & 0 & 0\\ 0 & -(L_{ls}+L_{md}) & 0 & 0 & L_{md} & L_{md}\\ -L_{mq} & 0 & (L_{lkq1}+L_{mq}) & L_{mq} & 0 & 0\\ -L_{mq} & 0 & L_{mq} & (L_{lkq1}+L_{mq}) & 0 & 0\\ 0 & -L_{md} & 0 & 0 & (L_{lfd}+L_{md}) & L_{md}\\ 0 & -L_{md} & 0 & 0 & L_{md} & (L_{lkd}+L_{md})\end{bmatrix}\begin{bmatrix}i^{r}_{qs}\\ i^{r}_{ds}\\ i'^{r}_{kq1}\\ i'^{r}_{kq2}\\ i'^{r}_{fd}\\ i'^{r}_{kd}\end{bmatrix} \quad (9)$$

The i^{r}_{qs} and i^{r}_{ds} are the stator currents in *dq* axes, the i'^{r}_{kq1}, i'^{r}_{kq2} and i'^{r}_{kd} are the rotor currents of three damper windings, and the i'^{r}_{fd} is the current of the field winding. The L_{md} and L_{mq} are the magnetizing inductances in *dq* axes, and the L_{ls} is the stator leakage inductance, while the leakage inductances of three damper windings are represented byL_{lkq1}, L_{lkq2} and L_{lkd}, and the field winding is represented by L_{lfd}.

The DG is connected to the VSC at BUS 2 via a step-up transformer with the ratio *a*. However, the transformers are assumed to be ideal for more accessible consideration. Therefore, the impedance (R_T and L_T) of the transformer can be ignored. It means $\frac{v_g}{a}=v_2$, which the v_g is the output voltage of DG at BUS G. The load currents at BUS 2 (i_{l2d} and i_{l2q}) can be derived. Where $v_{2d}=\frac{v^{r}_{ds}}{a}$ and $v_{2q}=\frac{v^{r}_{qs}}{a}$, the *a* is a step-up transformer ratio. The local load 2 resistance and inductance are represented by R_{l2} and L_{l2}, respectively, while the time constant $T_{l2}=\frac{R_{l2}}{L_{l2}}$.

$$\frac{di_{l2d}}{dt}=\frac{1}{L_{l2}}v_{2d}-\frac{1}{T_{l2}}i_{l2d}+\omega_r i_{l2q} \quad (10)$$

$$\frac{di_{l2q}}{dt}=\frac{1}{L_{l2}}v_{2q}-\frac{1}{T_{l2}}i_{l2q}-\omega_r i_{l2d} \quad (11)$$

2.2. Mathematical of MVDC

Although MVDC consists of two VSCs, this paper highlights the details of the VSC2. The paper's main objective is to implement power oscillation damping control at the DG, which can be achieved with the control at the VSC2. Therefore, in this paper, the details of the mathematical model of the VSC1 are not presented. The VSC2 has connected the DG ZONE at BUS V2 with interface impedance (R_{con2}, L_{con2} and C_{con2}). In addition, the R_{con2}, L_{con2} and C_{con2} are the RLC filter of the VSC2. The mathematical model of the VSC2 can be expressed as follows:

$$\frac{dv_{2d}}{dt}=-\frac{1}{C_{con2}}i_{l2d}-\frac{1}{C_{con2}}i_{con2d}+\frac{1}{C_{con2}}ai_{gd}+\omega_r v_{2q} \tag{12}$$

$$\frac{dv_{2q}}{dt}=-\frac{1}{C_{con2}}i_{l2q}-\frac{1}{C_{con2}}i_{con2q}+\frac{1}{C_{con2}}ai_{gq}-\omega_r v_{2d} \tag{13}$$

$$\frac{di_{con2d}}{dt}=-\frac{1}{T_{con2}}i_{con2d}+\frac{1}{L_{con2}}v_{2d}-\frac{1}{L_{con2}}v_{con2d}+\omega_r i_{con2q} \tag{14}$$

$$\frac{di_{con2q}}{dt}=-\frac{1}{T_{con2}}i_{con2q}+\frac{1}{L_{con2}}v_{2q}-\frac{1}{L_{con2}}v_{con2q}-\omega_r i_{con2d} \tag{15}$$

Where the $i_{gd}=i^r_{ds}$ and $i_{gq}=i^r_{qs}$. The i_{con2d} and i_{con2q} are the VSC2 currents on dq axes. The output voltages on dq axes of VSC2 are represented by v_{con2d} and v_{con2q} , respectively. The VSC2 output voltages can be expanded by $v_{con2d}=k_p u_{2d} v_{dc}$ and $v_{con2q}=k_p u_{2q} v_{dc}$. Whereas the v_{dc} is the DC voltage of the MVDC, and the k_p is a constant value of VSC. The control signal u_{2d} and u_{2q} can control the VSC2 output voltages. According to [22], showing the relation between AC power and DC power of the VSC, the power flow at the VSC2 can be derived as,

$$\frac{dv_{dc}}{dt}=\frac{1}{C_{dc2}R_{dc2}}v_{dc}-\frac{1}{C_{dc2}}i_{dc}-\frac{3}{2}\frac{1}{C_{dc2}}(u_{2d}i_{con2d}+u_{2q}i_{con2q}) \tag{16}$$

where C_{dc2} is the DC link capacitor, and the resistor R_{dc2} represents the loss in the VSC2. The i_{dc} is the DC current from the VSC1.

3. CONTROL SYSTEM AND DESIGN

The detail of distributed generator grid connection with MVDC and its controller is shown in Figure 4. As can be seen in this figure, the control system consists of two controllers: a VSC1 and VSC2 control. The functional control of the VSC1 regulates the DC voltage at DC BUS and controls the AC voltage at BUS V1. For the VSC2 control, the primary functional control is the AC voltage control at the load bus. Besides, the DG is connected to the system at this point, and the VSC2 is also used to control the power oscillation. Therefore, the VSC2 control consists of the AC voltage and the power oscillation controls. The detail of VSC1 and VSC2 controls can be expressed in the following sections.

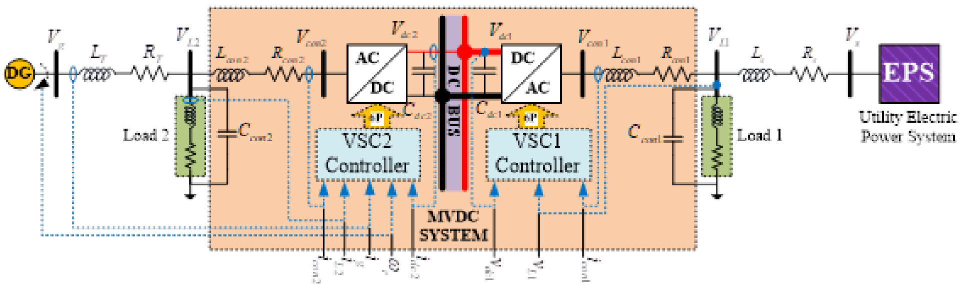

Figure 4. Detail of distributed generator grid connection with MVDC and its controller

3.1. Control strategy of the VSC1 and VSC2

The DC voltage is regulated by controlling the current on the d axis, while the AC voltage can be controlled by controlling the current on the q axis of the VSC1. The PI controllers are used to achieve those control functions, while the current control loop is successful using the hysteresis control. The DC and AC voltage control outputs are the reference currents on *dq* axes ($i^*_{con1,dq}$). Inverse Park transformation transform these currents to the *abc* axes [21]. The reference angle (θ) obtained from the phase-lock-loop (PLL) is applied in this process. The hysteresis current control compares the reference currents ($i^*_{con1,abc}$) with the feedback currents ($i_{con1,abc}$) to generate the switching six pulses for the VSC1. The detail of the VSC1 control diagram is shown in Figure 5(a).

In this paper, the local load 2 is connected to the system at the VSC2 zone. In addition, the DG has to connect to the system at this point. The AC load voltage control is necessary for VSC2. Moreover, installing the power oscillation damping control is added for VSC2 to enhance the power quality of the DG. The AC voltage control is achieved by controlling the current on the *q* axis, while the power oscillation damping control can be successful by controlling the current on the *d* axis. This paper proposes PINNF to control the AC voltage and damp the power oscillation. The outputs of the NN are the feed-forward reference currents on *dq* axes (i^*_{NNd} and i^*_{NNq}) . These currents are then combined with the PI controller's reference currents on *dq* axes ($i^*_{\omega d}$ and i^*_{Vd}). Similar to the VSC1, the total reference currents (i^*_{con2d} and i^*_{con2q}) are transformed to the *abc* axes using inverse Park transformation. The reference angle (θ_r) obtained from the rotor speed of DG will be applied in this process. The hysteresis current control compares the reference currents ($i^*_{con2,abc}$) with the feedback currents ($i_{con2,abc}$) to generate the switching six pulses for the VSC2. The detail of the VSC2 control diagram is shown in Figure 5(b).

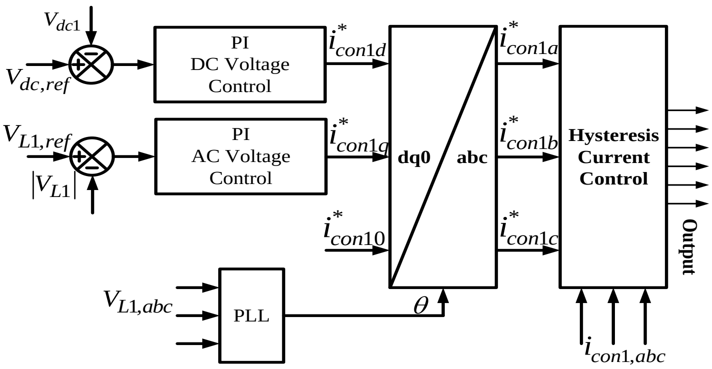

(a)

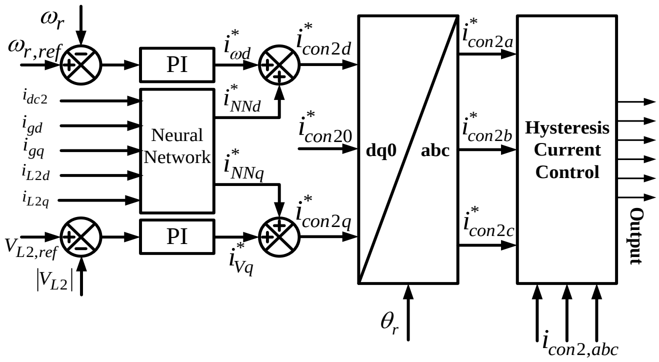

(b)

Figure 5. Diagram of VSC1 and VSC2 control (a) VSCI control and (b) VCS2 control

3.2. Control design

3.2.1. VSC1 controller design

Considering the connection network of VSC1 to the power system, as can be seen in Figure 4, it is found that the connection characteristics are similar to the connection of D-STATCOM devices to the power system. However, there is a difference that the VSC1 can exchange real power with the system. Therefore, the controller design process for D-STATCOM devices can be effectively applied to VSC1. This paper proposes the classical method called the loop shaping method [33] for tuning PI controllers of VSC1. By selecting the gain and phase margin of the control system, around 6.00 dB and 60.00 degrees, respectively, $K_{P,Vdc}$=-0.01, $K_{I,Vdc}$=-40.0 and $K_{P,Vac}$=-0.1, $K_{I,Vac}$=-2.0 are used. Where $K_{P,Vdc}$ and $K_{I,Vdc}$ are the P and I controller parameters of the DC voltage control, and $K_{P,Vac}$ and $K_{I,Vac}$ are the P and I controller parameters of the AC voltage control.

3.2.2. VSC2 controller design

The dynamic equations of the DG grid connection with the MVDC are shown in (1)-(7), (10)-(11), and (12)-(16). This paper uses the linear approximation technique [20] to study the system's dynamic behavior. A set of linear equations can be derived using the partial derivatives of the dynamic equations around an operating point (17).

$$\Delta x(t)=\left\{\frac{\partial f(x_0,u_0)}{\partial x}\right\}\Delta x(t)+\left\{\frac{\partial f(x_0,u_0)}{\partial u}\right\}\Delta u(t) \tag{17}$$

The (17) can be rewritten as,

$$\Delta\dot{x}(t)=A_0\Delta x(t)+B_0\Delta u(t) \tag{18}$$

where $\Delta x(t)$ and $\Delta u(t)$ are the state of the system and the control input, respectively. The state (or system) matrix A_0 and input matrix B_0 can be expressed in (19) and (20).

$$A_0=\left\{\frac{\partial f(x_0,u_0)}{\partial x}\right\} \tag{19}$$

$$B_0=\left\{\frac{\partial f(x_0,u_0)}{\partial u}\right\} \tag{20}$$

Then, the system's output $\Delta y(t)$ can be obtained, as shown in (21).

$$\Delta y(t)=C\Delta x(t)+D\Delta u(t) \tag{21}$$

Where C is the output matrix, and D is the feedthrough (or feed-forward) matrix. The multi-input-multi-output transfer function of the system can be obtained, as shown in (22).

$$G(s)=C(sI-A_0)^{-1}B_0+D \tag{22}$$

Where $G(s)$ is the multi-input-multi-output transfer function, and I is an identity matrix.

The system's dynamic performance can be obtained by using the transfer function in (22). The system's behavior depends on the operating point, and when the operating point is changed, the system's behavior will also be changed. Two variables: generator power and current of local load 2, can affect the system's behavior, as can be seen in Figures 6 and 7. An increase in the generator power under an improper excitation voltage condition will eventually lead to an unstable system corresponding to the roots and zeros of the system, as shown in Figure 6. In addition, the next point of concern is that excessive load currents can cause the system to become unstable. In this case, the roots and zeros of the system are shown in Figure 7.

For designing the VSC2 control system, the transfer function in (22) is used to determine the parameters of the PI controller. Similar to VSC1, the loop shaping method is also used for VSC2. The parameters of the PI controller are obtained by selecting the control system's gain and phase margin at nearly 6.00 dB and 60.00 degrees. The parameters of the PI controller of the AC voltage and the power oscillation damping controls are $K_{P,V}$=-0.3, $K_{I,V}$=30.0 and $K_{P,\omega}$=20,000, $K_{I,\omega}$=900,000, respectively. Where $K_{P,V}$ and $K_{I,V}$ are the P and I controller parameters of the AC voltage control, and $K_{P,\omega}$ and $K_{I,\omega}$ are the P and I controller parameters of the power oscillation damping control.

Although the proposed PI controller can be used to control AC voltage and power oscillations with good stability, the PI controller is a linear controller with good response and stability only around the design working point. Therefore, a sudden change of working point in a wide area can eventually lead to instability. In order to provide the VSC2 control with good response and stability in the broader area, this paper proposed a NN as a feed-forward controller in combination with the PI controller. The NN estimates a reasonable reference current for operating conditions and feeds it to the control system while the remaining control errors are eliminated with the PI controller. The next section will show the architecture and training process of neuron networks.

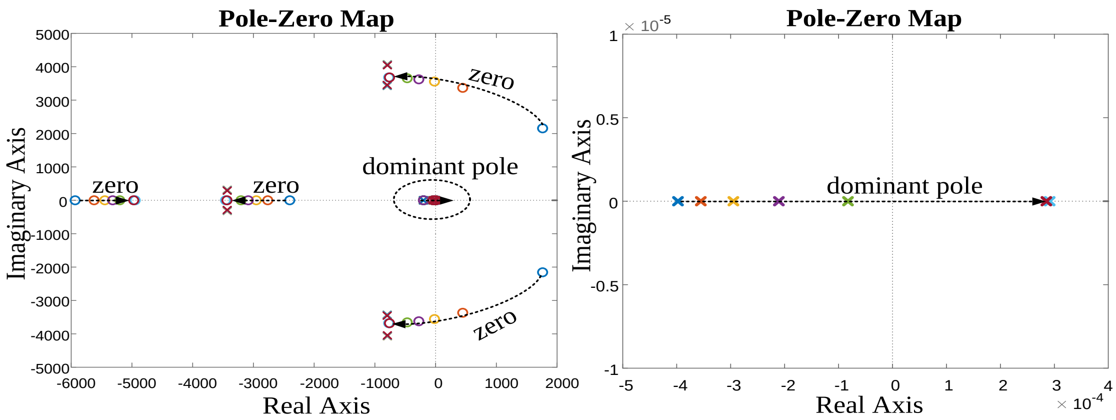

Figure 6. Roots and zeros of the system when increasing generator power

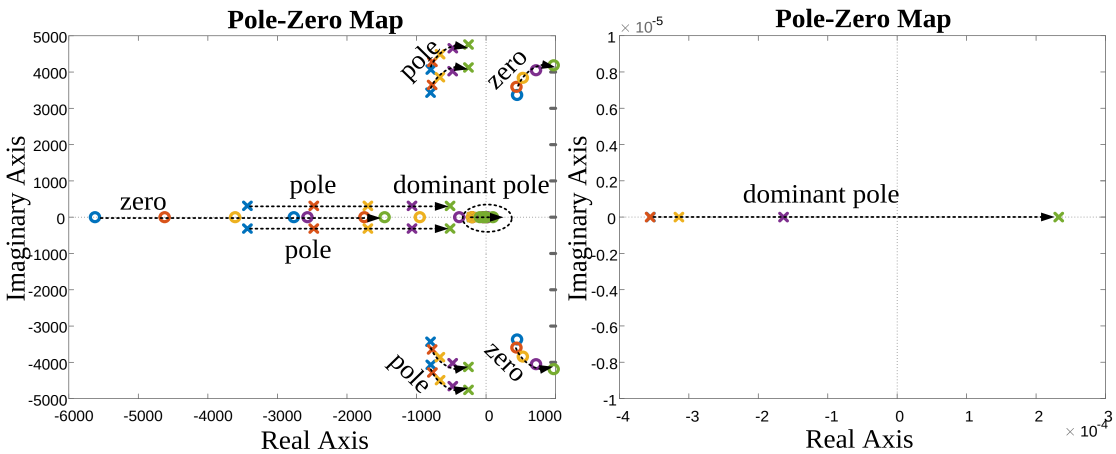

Figure 7. Roots and zeros of the system when increasing local load 2

3.3. Architecture and training process of neuron networks

The NN is usually composed of multiple neurons connected in parallel with a single or multiple layers. This paper used a two-layers (one-hidden layer and output layer) NN for model predictive to represent the plant's forward dynamics. The structure of the NN is shown in Figure 8. As shown in Figure 8, there are four neurons for the hidden layer and two for the output layer. The output in each layer can be written as in (23)-(24).

$$y_i^h = f^h(W_{i,j}^{in} p_i + b_i^h) \tag{23}$$

$$y_k^o = f^o(W_{i,k}^o y_i^h + b_k^o) \tag{24}$$

Where j and i are the j^{th} input and the i^{th} neuron of the hidden layer, respectively, and k is the k^{th} neuron of the output layer. The y_i^h and p_i are the output and input of the hidden layer, respectively. Meanwhile, the $W_{i,j}^{in}$ and b_i^h are weight matrix and bias matrix of the hidden layer, respectively. This paper uses the tan-sigmoid transfer function ($f^h = tansig(n_i^h)$) as a hidden layer transfer function when the n_i^h is the net input of the hidden layer. For the output layer, the output of the hidden layer y_i^h is used as the input, while the output is y_k^o. Meanwhile, the weight matrix and bias matrix are $W_{i,k}^o$ and b_k^o, respectively. The linear transfer function ($f^o = purelin(n_k^o)$) is an output layer transfer function when the n_k^o is the net input of the output layer.

The NN, in Figure 8 receives the state variables: i_{dc2}, i_{gd}, i_{gq}, i_{L2d} and i_{L2q} as the input and i_{con2d} and i_{con2q} as the targets derived from the mathematical model in section 2. Then the NN estimates the i_{NNd}^* and i_{NNq}^* through the transfer function. This paper uses the Levenberg-Marquardt Backpropagation algorithm for NN-based estimation. According to Levenberg-Marquardt method, the weight and bias variables are adjusted. The NN further estimates the i^*_{NNd} and i^*_{NNq} with updated weights and biases in the next step. This paper uses 500 data sets obtained from mathematical models under various conditions for the training process. The best NN training performance is shown in Figure 9.

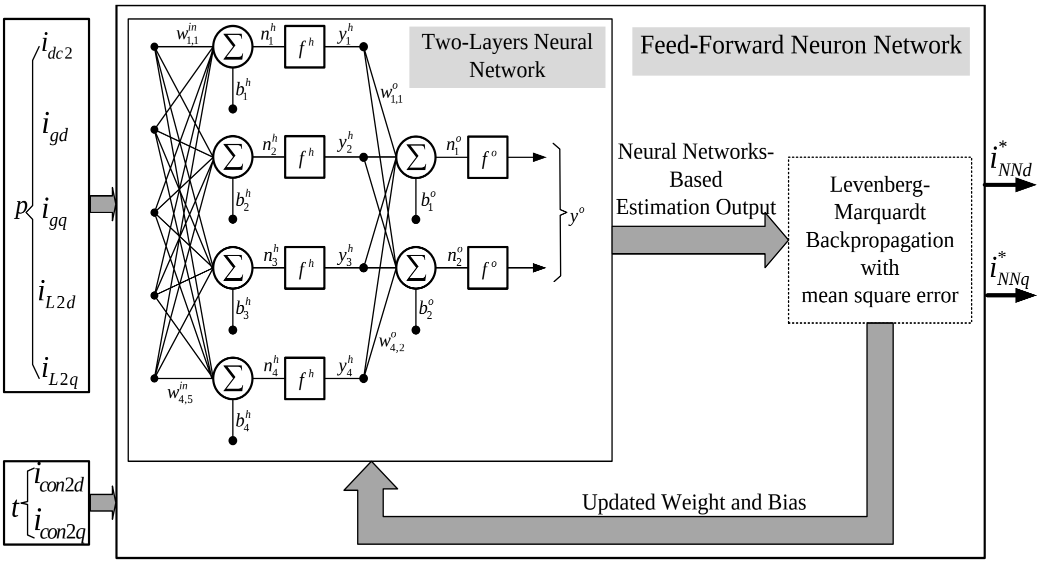

Figure 8. Architecture of the two-lawyers neural network for model predictive

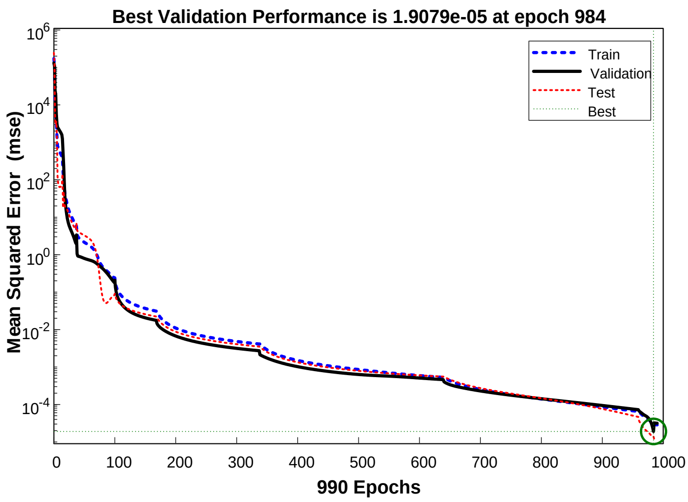

Figure 9. Neural network training performance

4. RESULTS AND DISCUSSIONS

This section presents and discusses comparing the proposed PINNF and the conventional PI controllers. The main objective of control is to solve power quality in power oscillation by connecting the DG to the distribution system with the MVDC. The test system and parameters are shown in Figure 10 and Table 1. The study is validated by simulation on the MATLAB/Simulink program. Among the four cases, case 1) the DG power (P_G) is increased from 0.5 MW to 2.8 MW of local load 2 power (P_{L2}) at a constant of 0.6 MW, case 2) the P_{L2} is increased from 0.6MW to 1.6 MW of P_G at a constant of 2.8 MW, case 3) the P_G is increased from 0.6 MW to 4.0 MW of P_{L2} at a constant of 1.6 MW, and case 4) the P_{L2} is increased from 0.6 MW to 1.6 MW of P_G at a constant of 4.0 MW.

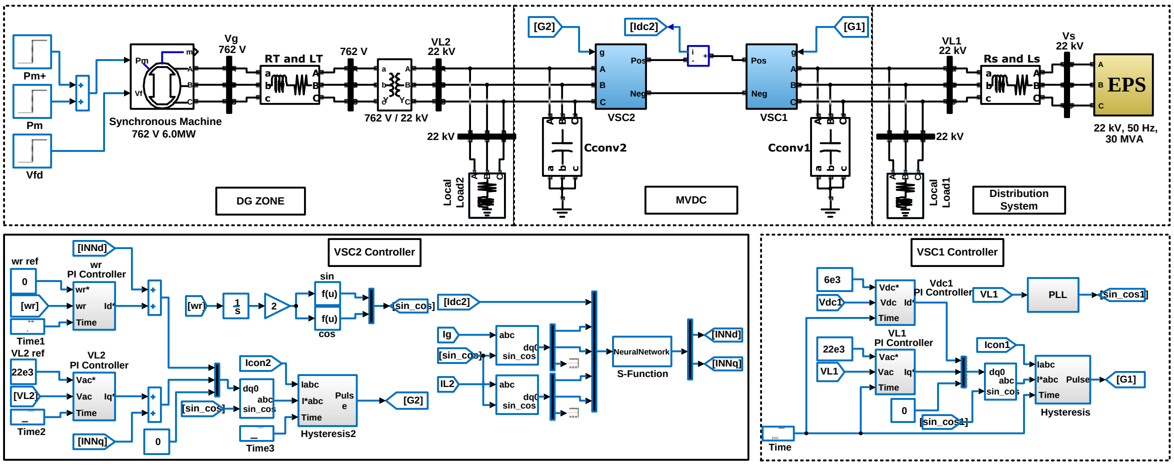

Figure 10. DG grid connection with MVDC and control on MATLAB/Simulink program

Table 1. Parameters of the test system

Test system	Parameters	Value
Distribution system	Nominal source voltage: V_s	22 kV
	Source and line resistance: R_s	0.1 Ω
	Source and line inductance: L_s	10 mH
	Nominal Local load1: $P_{L1} + jQ_{L1}$	$6 + j2$ MVA
DG Zone	Nominal power: P_m	5.0 MVA
	Nominal voltage: V_g	762 V
	Stator resistance and inductance: r_s, L_{ls}	0.078 Ω, 1.14 mH
	dq-axis magnetizing inductance: L_{md}, L_{mq}	13.7 mH, 11.0 mH
	Field resistance and inductance, r'_{fd}, L_{lfd}	0.13 Ω, 2.1 mH
	Damper d-axis resistance and leakage inductance: r'_{kd}, L_{lkd}	0.0224 Ω, 1.4 mH
	Damper q-axis resistance and leakage inductance: r'_{kq1}, L_{lkq1}	0.02 Ω, 1 mH
	Inertia coefficient: J	199.2 kg/m^2
	Friction factor: F	0.00 $N.m.s$
MVDC	Nominal DC voltage:	60 kV
	Interface impedance: R_{conv}, L_{conv}, C_{conv}	0.01 Ω, 0.1 mH, 100 μF
	DC capacitance, C_{dc}	2,000 μF
	Nominal Local load2: $P_{L2} + jQ_{L2}$	$4 + j0.6$ MVA

In case 1, the P_G increases from 0.5 MW to 2.8 MW at t = 1sec, while the P_{L2} is constant at 0.6 MW, as shown in Figure 11(a). As can be seen in this figure, the P_G is immediately increased and has the overshoots caused by the acceleration of the DG, while the P_{L2} is slightly affected. The response of P_{L2} is related to local load 2 bus voltage (V_{L2}). The V_{L2} is regulated at 22.00 kV, as shown in Figure 11(b). In this figure, the responses of the proposed PINNF and the conventional PI controller are similar in performance. The disturbance response of V_{L2} is increased due to an immediate increase in the P_G with the peak voltage of about 30.00kV, which the P_{L2} is slightly increased as well. And then, after about 40 msec, the PINNF and PI controllers have returned the V_{L2} to nearly 22.00 kV. Similarly, the P_{L2} is turning to the normal value. The peak voltage of the excursion is bounded by the P controller, while the I controller will eliminate the error until it is less than 100V (0.45%) in the steady-state. Generally, the rotor speed deviation of DG ($\Delta\omega_r$) can be affected by the P_G changes and may cause oscillation. Fortunately, the DG grid connection oscillation with MVDC and its control is rapidly settled, as shown in Figure 11(c). The disturbance response of $\Delta\omega_r$ is increased due to an immediate increase in the P_G with the peak of about 0.0005 p.u. and 0.0006 p.u. for the PINNF and PI controllers, respectively. Then, after about 70 msec, the PINNF and PI controllers have returned the $\Delta\omega_r$ to settle with about zero error in the steady-state. Furthermore, both the PINNF and PI control systems are stable. Although the proposed PINNF and the conventional PI control give similar responses, in this case, it is noticed that the PINNF gives slightly better results. It can be seen that the feed-forward signals of the PINNF controller show a slight improvement in the peak value and response time of the disturbance response of V_{L2} and $\Delta\omega_r$.

In case 2, the P_{L2} suddenly changed from 0.6 MW to 1.6 MW at t = 2 sec, while the P_G remains constant at 2.8 MW, as shown in Figure 12(a). The increased P_{L2} affects the load voltage V_{L2} to sag. However, the V_{L2} is regulated at the desired value of 22.00 kV by the MVDC and its control. The disturbance responses of V_{L2} are shown in Figure 12(b). As can be seen in this figure, the V_{L2} can reach the desired value within 10 msec for the proposed PINNF controller, while the conventional PI controller gives a slower response time at about 50 msec. In addition, the proposed PINNF controller shows a better sag voltage improvement than the conventional PI controller. The PINNF controller has a maximum sag voltage of about 2.00 kV (9.09%), while it is about 7.00 kV (31.82%) of the PI controller. Similarly, to the V_{L2}, the increased P_{L2} also affects $\Delta\omega_r$ as shown in Figure 12(c). In this case, it seems that the DG has been interrupted and is trying to return to the normal operating point by accelerating and decelerating the speed of the DG; this causes the DG's power to oscillate, or the $\Delta\omega_r$ oscillation. If the DG connects to the system with traditional AC distribution networks, the oscillation can take several seconds or even minutes, adversely affecting the power system. However, this oscillation can be better improved by using MVDC, especially under the proposed PINNF controller. The maximum oscillation is limited at 0.0001 p.u. and 0.0005 p.u. for the PINNF and PI controllers, respectively. In addition, the PINNF controller gives a fast time response to the settling $\Delta\omega_r$ of about 10 msec, the PI controller has a time response of about 100 msec. However, the PINNF and PI controllers can also eliminate the steady-state error to zero with stable systems. In this case, the simulation results showed that the proposed PINNF controller provided significantly better performance than the PI controller, which means the PINNF controller shows greater performance in the disturbance response of V_{L2} and $\Delta\omega_r$ and nonlinear systems handling.

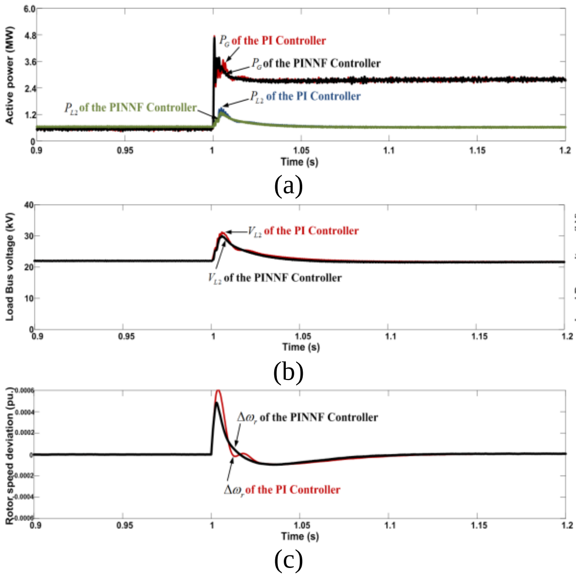

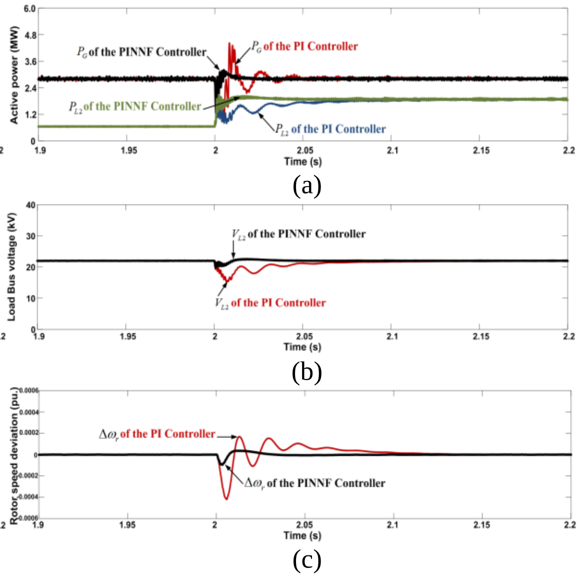

Figure 11. The P_G increases from 0.5MW to 2.8MW of the P_{L2} at a constant of 0.6MW for (a) active powers at the DG and local load, (b) the load bus voltage, and (c) the rotor speed deviation

Figure 12. The P_{L2} increases from 0.6MW to 1.6MW of the P_G remains constant at 2.8MW for (a) active powers at the DG and local load, (b) the load bus voltage, and (c) the rotor speed deviation

In case 3, the P_G increases from 0.5 MW to 4.0 MW, while the P_{L2} constant at 0.6MW is tested at time t = 1sec, as seen in Figure 13(a). In this case, a relatively higher increase in power results in a high nonlinear system. This substantial increase in power (about 8 times) brings the system closer to the region of instability, as seen from the analysis of the roots path of the system in Figure 6. The DG has highly increased the power that highly affects the load voltage V_{L2} and rotor speed deviation $\Delta\omega_r$. The disturbance responses of V_{L2} in this case, are shown in Figure 13(b). The PINNF and PI controllers can regulate the V_{L2} at the desired value within 40 msec under a steady-state error of less than 100V (0.45%) with the stable system. However, the PI controller's response shows two waves of the peak voltage at about 35.00 kV, whereas the PINNF shows only one peak voltage. It means that the PINNF controller can eliminate the disturbance response of V_{L2} better than the PI controller. Figure 13(c) presents the responses of the $\Delta\omega_r$. As seen in this figure, the simulation results show that the PINNF controller reveals a better response than that of the PI controller, with the peak of the $\Delta\omega_r$ of 0.0015 p.u. and 0.0016 p.u for the PINNF and PI controllers, respectively. And the $\Delta\omega_r$ are settled within about 20 msec for the PINNF, while the PI controller is about 40 msec. However, in this case, the PINNF and PI controllers can also eliminate the steady-state error to zero with stable systems.

In the last case, case 4, the P_{L2} is increased from 0.6MW to 1.6MW at time t = 2sec, while the P_G is constant at 4.0MW, as presented in Figure 14(a). In this case, the system has operated near the critical point, which is highly sensitive to changes. Although the increased power P_{L2} in this case is the same as in case 1, the system operates near the critical point, so it is susceptible to power changes. This results in a sharp sag voltage V_{L2}. So, the PI controller cannot control this voltage (unstable system), as seen in Figure 14(b). However, with the PINNF controller, the NN estimates a reasonable reference current for operating conditions and feeds it to the control system, which can regulate the V_{L2} at the desired value within 10 msec with a small sag voltage of about 2.00 kV. Moreover, the system with the PINNF controller shows a less steady-state error than 100V (0.45%) with stability. In this case, the responses of the $\Delta\omega_r$ are presented in Figure 14(c). As can be noticed in this figure, the simulation results show that the PINNF controller can improve the oscillation of the $\Delta\omega_r$ to settle within about 10 msec with the steady-state error to zero, while the PI controller cannot control the $\Delta\omega_r$ with an unstable system.

The graphics analysis has revealed that the proposed PINNF controller approach has yielded far more favorable results than the conventional PI controller. It has been observed that the PI controller is unsuitable for controlling such that the system operates near the critical point. On the other hand, the system remains stable when using the PINNF controller, and the oscillations are quickly settled. It can be concluded that the proposed PINNF controller provides better performance, mainly when the system operates near the critical point and high nonlinear system.

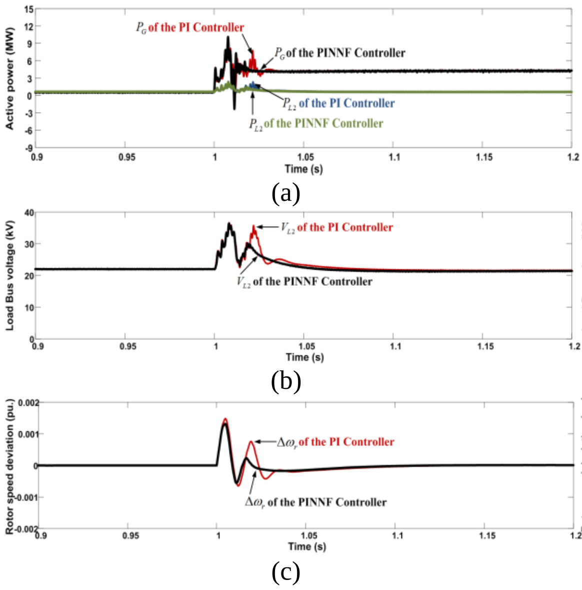

Figure 13. The P_G increases from 0.5MW to 4.0 MW, while the P_{L2} is constant with 0.6MW for (a) active powers at the DG and local load, (b) the load bus voltage and (c) the rotor speed deviation

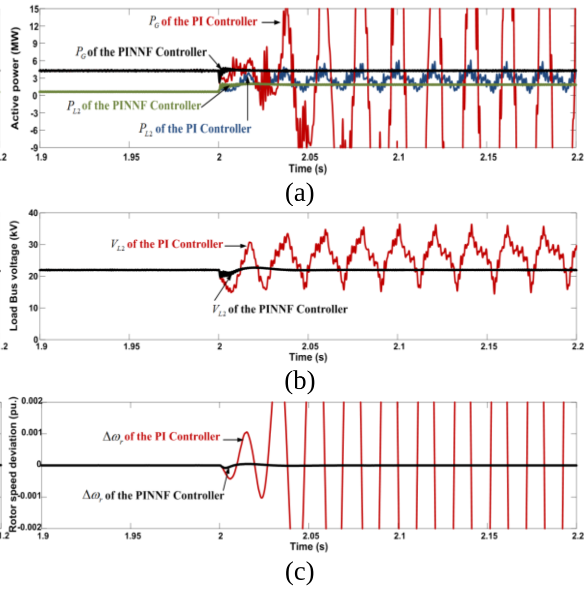

Figure 14. The P_{L2} is increased from 0.6MW to 1.6 MW, while the P_G is constant with 4.0MW for (a) active powers at the DG and local load, (b) the load bus voltage and (c) the rotor speed deviation

5. CONCLUSION

This paper presented the connection of the DG to the distribution system with MVDC. The advantages of MVDC are obtained. Examples are the possibility of quickly controlling the constant AC voltage on both sides of the DG and distribution system and improving power quality in significantly mitigating power oscillations. In this paper, the main objective of the MVDC is to improve power oscillation at the connection point of the DG to remain in synchronism. It can continuously supply power to the system in every possible change, such as the increased DG power and local load power. The results of two controllers, the proposed PINNF and the conventional PI controllers, are compared and discussed. The results of four cases confirm that the MVDC could improve the power oscillation. It is also found that the MVDC with the proposed PINNF controller gives a better response than the conventional PI controller, especially in cases where the system is susceptible to working point change. The proposed PINNF control performs well and can handle high nonlinear systems because the NN as a feed-forward path can estimate the proper reference currents in each situation to the control system. In addition, the feed-forward path is outside the loop and thus does not respond to disturbances leading to a better performance of the PINNF controller.

REFERENCES

[1] N. Md. Saad, M. Z. Sujod, Lee Hui Ming, F. Abas, M. S. Jadin, M. R. Ishak and N. R. H. Abdullah, "Impacts of photovoltaic distributed generation location and size on distribution power system network," *International Journal of Power Electronics and Drive System (IJPEDS)*, vol. 9, no. 2, pp. 905-913, 2018, doi: 10.11591/ijpeds.v9.i2.pp905-913.

[2] P. S. Georgilakis and N. D. Hatziargyriou, "Optimal distributed generation placement in power distribution networks: models, methods, and future research," *IEEE Transactions on Power Systems*, vol. 28, no. 3, pp. 3420-3428, Aug. 2013, doi: 10.1109/TPWRS.2012.2237043.

[3] S. Bifaretti, P. Zanchetta, A. Watson, L. Tarisciotti and J. C. Clare, "Advanced power electronic conversion and control system for universal and flexible power management," *IEEE Transactions on Smart Grid*, vol. 2, no. 2, pp. 231-243, 2011, doi: 10.1109/TSG.2011.2115260.

[4] Z. Huang *et al*., "Research status and prospect of control and protection technology for DC distribution network," in *China International Conference on Electricity Distribution (CICED)*, 2014, pp. 1488-1493, doi: 10.1109/CICED.2014.6991953.

[5] Y. Leukhampeng, P. Sanpoung and K. Somsai, "Application of D-STATCOM for voltage sag mitigation and power oscillation damping," in *International Conference on Electrical Engineering/Electronics, Computer, Telecommunications and Information Technology (ECTI-CON)*, 2021, pp. 810-815, doi: 10.1109/ECTI-CON51831.2021.9454805.

[6] T. Shintai, Y. Miura and T. Ise, "Oscillation Damping of a distributed generator using a virtual synchronous generator," in *IEEE Transactions on Power Delivery*, vol. 29, no. 2, pp. 668-676, 2014, doi: 10.1109/TPWRD.2013.2281359.

[7] A. U. Krismanto, N. Mithulananthan and I. Kamwa, "Oscillatory stability assessment of microgrid in autonomous operation with uncertainties," *IET Renewable Power Generation*, vol 12, no. 4, pp. 494-504, 2018, doi: 10.1049/iet-rpg.2017.0579.

[8] G. Rogers, *Power System Oscillations*, New York, NY, USA: Springer New York, 2000.

[9] Y. Xing, B. Marinescu, M. Belhocine and F. Xavier, "Power oscillations damping controller for HVDC inserted in meshed AC grids," *IEEE PES Innovative Smart Grid Technologies Conference Europe (ISGT-Europe)*, 2018, pp. 1-6, doi: 10.1109/ISGTEurope.2018.8571732.

[10] O. Saborio-Romano, A. Bidadfar, O. Göksu, L. Zeni and N. A. Cutululis, "Power oscillation damping from offshore wind farms connected to HVDC via diode rectifiers," *Energies*, vol. 12, no. 17, pp. 1-15, 2019, doi: 10.3390/en12173387.

[11] M. M. A. Hassan, X. Sun and A. Ate, "FLC based on static var compensator for power system transient stability enhancement," *TELKOMNIKA Telecommunication, Computing, Electronics and Control*, vol 18, no. 5, pp. 2665-2673, 2020, doi: 10.12928/TELKOMNIKA.v18i5.15605.

[12] M. M. Eissa, *Medium-Voltage Direct Current Grid: Resilient Operation, Control and Protection*, UK: Academic Press, 2019.

[13] J. Yu, K. Smith, M. Urizarbarrena, M. Bebbington, N. Macleod and A. Moon, "Initial designs for angle-DC project: challenges converting existing ac cable and overhead line to dc operation," *Proceedings of the CIRED*, 2017, pp. 12–15, doi: 10.1049/oap-cired.2017.0974.

[14] L. Qu *et al*., "Planning and analysis of the demonstration project of the MVDC distribution network in Zhuhai," *Front. Energy*, vol 13, no. 1, pp. 120-130, 2019, 10.1007/s11708-018-0599-2.

[15] Working Group C6.31, "Medium voltage direct current (MVDC) grid feasibility study," in *ELECTRA CIGRE's Digital Magazine*, 2020, no. 309, pp. 1–5. [online]. Available: https://electra.cigre.org/309-april-2020/technical-brochures/medium-voltage-direct-current-mvdc-grid-feasibility-study.html. Accessed on 11 March 2022.

[16] T. Joseph, J. Liang, G. Li, A. Moon, K. Smith and J. Yu, "Dynamic control of MVDC link embedded in distribution network: — Case study on ANGLE-DC," in *IEEE Conference on Energy Internet and Energy System Integration (EI2)*, 2017, pp. 1-6, doi: 10.1109/EI2.2017.8245752.

[17] R. Bernacchi, "MVDC and grid interties: enabling new features in distribution, sub-transmission and industrial networks," *ABB: Zurich*, Switzerland, 2019.

[18] D. Kumar, F. Zare and A. Ghosh, "DC microgrid technology: system architectures, AC grid interfaces, grounding schemes, power quality, communication networks, applications, and standardizations aspects," *IEEE Access*, vol. 5, pp. 12230-12256, 2017, doi: 10.1109/ACCESS.2017.2705914.

[19] M. Ahmed, A. Vahidnia, M. Datta and L. Meegahapola, "An adaptive power oscillation damping controller for a hybrid AC/DC microgrid," *IEEE Access*, vol. 8, pp. 69482-69495, 2020, doi: 10.1109/ACCESS.2020.2985978.

[20] J. D'Azzo and H. Houpis, *Linear control system analysis and design: conventional and modern*, Mc. Graw-Hill, 1995.

[21] F. Blaabjerg, *Control of Power Electronic Converters and Systems*, Academic Press, 2021.

[22] K. Somsai, "Controller design of UPQC for enhancing power quality in distribution system," in *International Journal of Power Electronics and Drive System (IJPEDS)*, vol. 9, no. 4, pp. 1591-1606, 2018, doi: 10.11591/ijpeds.v9.i4.pp1591-1606.

[23] F. Mehmood, S. Maqsood, R. Damaševičius and T. Blažauskas, "Disturbance rejection and control design of MVDC converter with evaluation of power loss and efficiency comparison of SiC and Si based power devices," *Electronics*, vol. 9 no. 1878, pp. 1-25, 2020, doi: 10.3390/electronics9111878.

[24] M. Muruganandam and M. Madheswaran, "Stability analysis and implementation of chopper fed DC series motor with hybrid PID-ANN controller," *International Journal of Control, Automation, and Systems*, vol. 11, no. 5, pp. 966-975, 2013, doi: 10.1007/s12555-012-9209-y.

[25] W. Wang, A. Beddard, M. Barnes and O. Marjanovic, "Analysis of active power control for VSC–HVDC," *IEEE Transactions on Power Delivery*, vol. 29, no. 4, pp. 1978-1988, 2014, doi: 10.1109/TPWRD.2014.2322498.

[26] C. Guo, J. Liu, X. Guo, D. Zhu and X. Zou, "Feedforward compensation control for variable voltage and variable frequency voltage source converter," in *IEEE International Electrical and Energy Conference (CIEEC)*, 2021, pp. 1-5, doi: 10.1109/CIEEC50170.2021.9510608.

[27] O. Y. Her, M. S. A. Mahmud, M. S. Z. Abidim, R. Ayop and S. Buyamin, "Artificial neural network based short term electrical load forecasting," *International Journal of Power Electronics and Drive System (IJPEDS)*, vol. 13, no. 1, pp. 586-593, 2022, doi: 10.11591/ijpeds.v13.i1.pp586-593.

[28] S. Kanata, G. H. M. Sianipar and N. U. Maulidevi, "Optimization of reactive power and voltage control in power system using hybrid artificial neural network and particle swarm optimization," in *International Conference on Applied Electromagnetic Technology (AEMT)*, 2018, pp. 67-72, doi: 10.1109/AEMT.2018.8572408.

[29] C. Xie, S. Quan and Q. Chen, "Control strategy of hybrid power system for fuel cell electric vehicle based on neural network optimization," *IEEE International Conference on Automation and Logistics*, 2008, pp. 753-757, doi: 10.1109/ICAL.2008.4636250.

[30] I. Sudiharto, F. D. Murdianto and A. Wulandari, "Adaptive charging control using ANN-PID controllers on multiple DC loads with varying battery voltages," *International Journal of Power Electronics and Drive System (IJPEDS)*, vol. 13, no. 1, pp. 620-630, 2022, doi: 10.11591/ijpeds.v13.i1.pp620-630.

[31] H. Lee, S. Jhang, W. K. Yu, J. H. Oh, "Artificial neural network control of battery energy storage system to damp-out inter-area oscillations in power systems," *Energies*, vol. 12, no. 3372, pp. 1-13, 2019, doi: 10.3390/en12173372.

[32] R. T. Smith, *Analysis of Electrical Machines*, Pergamon Press, 1982.

[33] K. Somsai, N. Voraphonpiput, T. Kulworawanichpong, "Loop shaping control of distribution STATCOM," *International Journal of Control and Automation*, vol. 6, no. 1, pp. 87-103, 2013.

BIOGRAPHY OF AUTHORS

Kittaya Somsai is currently an assistant professor in the Department of Electrical Engineering, Rajamangala University of Technology Isan (RMUTI) Sakon Nakhon Campus, Thailand. He received the B.Eng in Electrical Engineering from Rajamangala's Institute of Technology, Thailand (2003), M.Eng in Electrical Engineering from King Mongkut's Institute of Technology North Bangkok (KMITNB), Thailand (2005), and Ph.D. in Electrical Engineering from Suranaree University of Technology, Thailand (2012). His research fields are interested in power systems, custom power devices, power electronics and control, and artificial intelligence techniques. He can be contacted at email: kittaya.so@rmuti.ac.th.

Nakarin Sripanya is a lecturer of the Department of Electrical Engineering, Rajamangala University of Technology Isan (RMUTI) Sakon Nakhon Campus, Thailand. He received the B.Ind.Tech in Electronics Engineering from North Eastern University (NEU), Thailand (2002), M.I.Ed. in Electrical Engineering from King Mongkut's University of Technoglogy Thonburi (KMUTT), Thailand (2006). His fields of research are embedded systems and automation systems. He can be contacted at email: nakarin.sr@rmuti.ac.th.

Chaiyut Sumpavakup received the BE, ME, and Ph.D. degrees in Electrical Engineering from Suranaree University of Technology, Thailand, in 2005, 2008, and 2017. He is currently an assistant professor in the Department of Power Engineering Technology, College of Industrial Technology, King Mongkut's University of Technology North Bangkok, Thailand. His research interests are electric railway systems, electric vehicles, and artificial intelligence techniques. He can be contacted at email: chaiyut.s@cit.kmutnb.ac.th.